# Magnetic cannon: The physics of the Gauss rifle

Arsène Chemin, Pauline Besserve, Aude Caussarieu, Nicolas Taberlet, and Nicolas Plihon[a)]
*Univ. Lyon, Ens de Lyon, Univ. Claude Bernard, CNRS, Laboratoire de Physique, F-69342 Lyon, France*

(Received 6 July 2016; accepted 9 March 2017)

The magnetic cannon is a simple device that converts magnetic energy into kinetic energy. When a steel ball with low initial velocity impacts a chain consisting of a magnet followed by addition steel balls, the last ball in the chain gets ejected at a much larger velocity. The analysis of this spectacular device involves an understanding of advanced magnetostatics, energy conversion, and the collision of solids. In this article, the phenomena at each step of the process are modeled to predict the final kinetic energy of the ejected ball as a function of a few parameters that can be experimentally measured. © *2017 American Association of Physics Teachers.*
[http://dx.doi.org/10.1119/1.4979653]

## I. INTRODUCTION

### A. What is a magnetic cannon?

The magnetic cannon, sometimes referred to as the Gauss rifle, is a simple device that accelerates a steel ball through conversion of magnetic energy into kinetic energy.[1–4] The energy conversion at work is reminiscent of other electromagnetism-based accelerating devices such as railguns.[5] Figure 1 shows a time sequence (from top to bottom) of a typical setup, where a line of four balls, the first of which is a permanent magnet, are impacted on the left by another steel ball. (The balls are sitting on a rail so the motion is constrained to one dimension.)

When the additional ball approaches from the left with a low initial velocity, it experiences an attractive magnetic force, collides with the magnet, and then the rightmost ball is ejected at a high velocity. To highlight the various features in Fig. 1, note that the frames are not equally spaced in time. The video from which these frames have been extracted is available as an online enhancement to Fig. 1.

To understand the physics of the Gauss rifle, the process may be divided into three phases: (i) acceleration of the ferromagnetic steel ball in the magnetic field created by the magnet (frames I–III in Fig. 1), (ii) momentum propagation into the chain of steel balls, similar to the momentum propagation in Newton's cradle (frame IV), and (iii) ejection of the final ball escaping the residual magnetic attraction (frames V and VI). While Fig. 1 highlights a specific example, we will focus on the more general case shown schematically in Fig. 2, where the initial chain is formed of $n$ steel balls in front of the magnet and $m$ balls behind (each ball having mass $M$ and radius $R$). The magnet is a strong NdFeB permanent magnet that is affixed to the rail, strongly enough to prevent the chain from moving in the leftward direction during the acceleration phase, but loosely enough to allow momentum propagation in the chain (a patch of putty can be observed in Fig. 1). Note that the dipolar axis of the magnet will spontaneously align with the axis of the chain to minimize potential energy.

The acceleration phase is governed by the magnetic field created by the magnet[6,7] and the magnetization of the impacting steel ball. The determination of the magnetization of the incoming ferromagnetic steel ball differs from classical problems in which the material (dia- or para-magnetic balls[8]) or geometry (large sample of ferromagnetic materials[9–11]) are different from ours. The acceleration of the impacting ball is related to the magnetic energy $U_n$, which depends on the number $n$ of balls screening the magnetic field of the magnet. Part of this magnetic energy is converted into kinetic energy, which adds to the initial kinetic energy $K_{\text{init}}$ of the incoming ball, and results in an impacting kinetic energy $K_{\text{impact}}$. The energy transfer in the chain is reminiscent of Newton's cradle,[12,13] and governed by Hertzian contact forces involving dissipation[14] in an inhomogeneous chain containing a magnet. Part of the impacting energy is transmitted through the chain, resulting in a kinetic energy $K_{\text{eject}}$ of the ejected ball. Finally, during the expulsion phase, the ejected ball loses energy while escaping the residual magnetic attraction $U_{m-1}$ on the right side of the chain, resulting in a final kinetic energy $K_{\text{final}}$.

The goal of the present article is to relate $K_{\text{final}}$ to $K_{\text{init}}$ and the parameters of the system. Note that the energy conversion process in this problem is not in contradiction with the fact that magnetic fields do no work on charged particles (the Lorentz force being perpendicular to the charged particle's velocity). The analysis of a situation similar to the one investigated here is discussed in detail in Griffiths's textbook,[15] and interested readers should also refer to the discussion about magnetic energy provided in Jackson's textbook[16] (from p. 224 onwards). In this article, effects related to the conversion of magnetic energy into kinetic energy are discussed in Sec. II. The transmission of kinetic energy through the chain is then detailed in Sec. III. Finally, parameters influencing the global energy conversion of the system and the understanding of a succession of Gauss rifles are discussed in Sec. IV.

### B. What students can learn from this problem

At an introductory physics level, this experiment can be used to foster a student's motivation while working on an open problem involving energy conservation. In a more traditional laboratory, students could use their knowledge of magnetism to determine whether the incoming steel ball should be considered as a permanent or an induced magnet through magnetic force and magnetic field measurements. At a graduate level, the question of the dependence of the final velocity on some of the parameters of the system might lead to an experimental project in which knowledge of mechanics, magnetism, and nonlinear physics come into play.

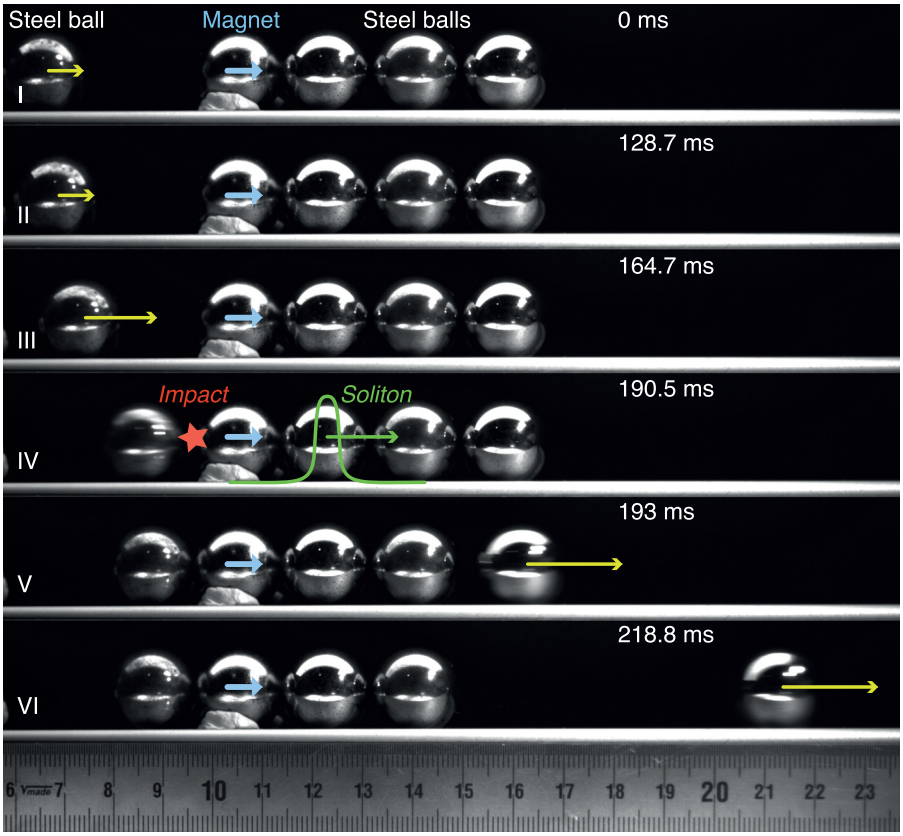


Fig. 1. (Color online) Time sequence (from top to bottom) showing the different phases of the magnetic cannon. A chain of three steel balls initially stuck to the right of a strong permanent magnet (loosely fixed on a rail with putty) is impacted by a steel ball coming from the left and accelerated in the magnetic field of the magnet. Momentum is transferred through the chain and the last ball on the right is ejected with a high velocity. The images are from a high-speed video (resolution: 2048 × 360) acquired at 400 frames per second (enhanced online) [URL: http://dx.doi.org/10.1119/1.4979653.1].

## II. FROM MAGNETIC ENERGY TO KINETIC ENERGY

In this section, we investigate the conversion of magnetic energy $U_n$ into kinetic energy in the acceleration phase, as well as the symmetric problem of the decrease of kinetic energy by $U_{m-1}$ in the ejection phase. Direct measurement of the spatial dependence of the magnetic force exerted by the magnet on the incoming (ejected) ball and of the magnetic field is in agreement with a permanent dipole/induced dipole modeling.

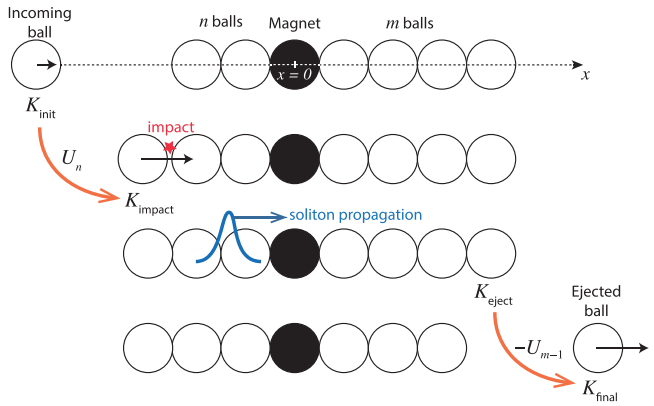


Fig. 2. Schematic of the sequences described in Fig. 1 and associated kinetic energy $K$ and (potential) magnetic energy $U$. The arrows represent conversion between magnetic energy and kinetic energy.

### A. Force exerted by the chain on a steel ball: A permanent/induced dipole interaction

Let us first focus on the direct measurement of the magnetic force exerted on the steel ball. Its spatial dependence is measured using a precision weight scale as sketched in Fig. 3. A steel ball is attached to a heavy plastic block resting on the scale below the magnetic cannon chain. The steel ball attached to the scale is subject to its weight in the downward direction and to a magnetic force in the upward direction. The force exerted by the magnet as a function of the distance $d$ between the center of the ball attached to the scale and the center of the magnet, derived from the (measured) apparent mass, is displayed in Fig. 3. We observe that in the presence of one or two steel balls in front of the magnet, the force is

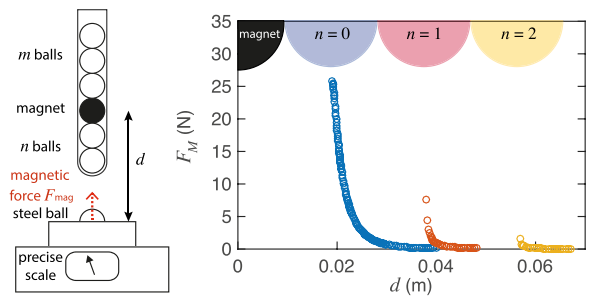


Fig. 3. Force measurement setup and spatial dependence of the magnetic force experienced by the steel ball attached to the scale as a function of the number $n$ of steel ball in front of the magnet.

screened but is nonetheless larger than it would have been with a chain of non-magnetic balls, since the ferromagnetic balls channel the magnetic field. A second observation, not illustrated here, is that the number of balls behind the magnet has no noticeable influence on the force exerted on the opposite side.

We will now establish the relation between this magnetic force and the magnetic field created by the magnet, in a way similar to that developed by Jackson,[17] and show that the permanent/induced dipole assumption is accurate. The measured intensity of the field, along the magnet's axis as a function of the distance $d$ from its center is shown in Fig. 4. The magnetic field intensity was measured using a Bell 7030 Gaussmeter but could also be measured using other integrated electronic devices.[18] As seen in the figure, the field scales as $d^{-3}$ as expected for the magnetic field outside a uniformly magnetized sphere.[16] The dipole strength of the magnet, $M_0$, can be determined according to

$$B(d) = \frac{\mu_0 M_0}{2\pi d^3}, \tag{1}$$

where $\mu_0$ is the vacuum magnetic permeability. The best fit according to Eq. (1) up to $d \sim 0.2$ m is shown as full black lines in Fig. 4 and leads to the value $M_0 = 3.64 \pm 0.1$ A m$^2$. Note that this best dipolar approximation slightly overestimates the magnetic field in the close vicinity of the magnet, as shown in Fig. 4.

The origin of the magnetic force experienced by the ferromagnetic steel ball lies in the interaction of the magnetic field created by the magnet and the magnetization of the steel ball. Assuming that the steel ball has an induced magnetic moment $\mathbf{m}_{\text{ball}}(d)$, the force reads

$$\mathbf{F}_{\text{M}}(d) = -\nabla(\mathbf{m}_{\text{ball}}(d) \cdot \mathbf{B}(d)). \tag{2}$$

This equation clearly shows a dependence on the magnetization properties of the steel ball. If $\mathbf{m}_{\text{ball}}(d)$ is constant and independent of $d$ (i.e., the steel is at saturation), then $F_{\text{M}}(d)$ is expected to scale as $d^{-4}$ as for an interaction between permanent dipoles.[6] On the other hand, if $\mathbf{m}_{\text{ball}}(d) \propto \mathbf{B}(d)$, then $F_{\text{M}}(d)$ is expected to scale as $d^{-7}$ as for an interaction between a permanent dipole and an induced dipole.

The experimental data shown in Fig. 3 are displayed on logarithmic scales in Fig. 5 and are consistent with a $d^{-7}$ scaling when $n = 0$. This justifies the hypothesis of an induced magnetization proportional to the magnetic field, or equivalently a permanent/induced dipole interaction. A precise computation of the ball magnetization is a rather difficult task, since the field is highly inhomogeneous over the ball volume and the (unknown) magnetic permeability of the steel is expected to play a leading role. However, as we will show, a simple model correctly describes our experimental data.

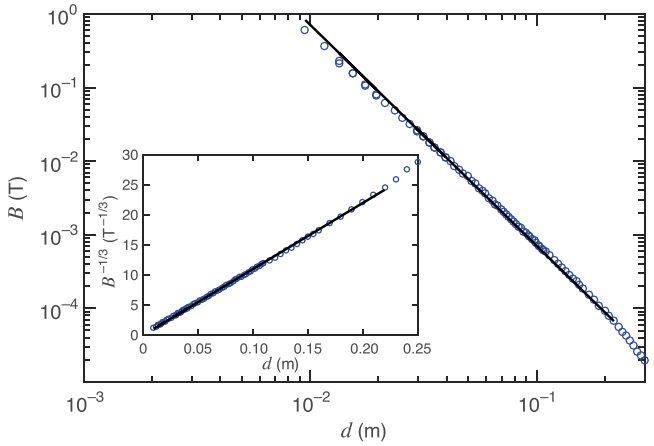


Fig. 4. Spatial dependence of the magnetic field created by the magnet shows a $1/d^3$ behavior; the inset shows $B^{-1/3}(d)$. The solid lines represent the associated best fits for a dipolar field.

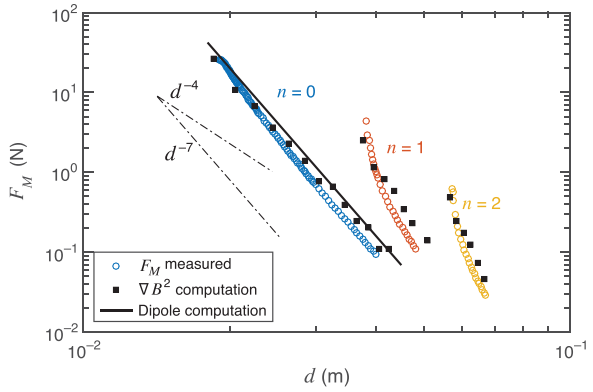


Fig. 5. Spatial dependence of the magnetic force for $n = 0$, 1, and 2: direct force measurements (open circles), force computed from magnetic field measurements according to Eq. (4) (black squares), and according to Eq. (5) for $n = 0$ (a solid line), showing the validity of our permanent/induced dipole model.

Let us first recall a classical result of magnetostatics[16]—the magnetic moment of a sphere of relative magnetic permeability $\mu_r$ immersed in a constant and homogeneous magnetic field $\mathbf{B}_0$ is given by

$$\mathbf{m}_{\text{ball}} = \frac{4\pi R^3}{3\mu_0}\frac{3(\mu_r - 1)}{\mu_r + 2}\mathbf{B}_0, \tag{3}$$

leading to a magnetic field intensity inside the ball of $3\mu_r B_0/(\mu_r + 2)$. In other words, the magnetic field is amplified inside the sphere by a factor $3\mu_r/(\mu_r + 2)$. In the case of soft steel, one expects values of $\mu_r$ in the range of 50–10,000, which leads to a maximum three-fold increase. Let us make a crude approximation and now assume that Eq. (3) remains valid in our configuration where the magnetic field created by the magnet is strongly inhomogeneous. Using the value of the magnetic field at the center of the steel ball, this leads to the following approximation of the magnetic force experienced by the steel ball:

$$F_{\text{M}}(d) = -\frac{4\pi R^3}{\mu_0}\frac{\mu_r - 1}{\mu_r + 2}\frac{\partial B^2}{\partial d} \underset{\mu_r \gg 1}{\approx} -\frac{4\pi R^3}{\mu_0}\frac{\partial B^2}{\partial d}. \tag{4}$$

Using the dipolar model for the magnetic field given in Eq. (1), the force can be conveniently expressed as

$$F_{\text{M}}(d) = \frac{6\mu_0 R^3 M_0^2}{\pi d^7}\frac{\mu_r - 1}{\mu_r + 2} \underset{\mu_r \gg 1}{\approx} \frac{6\mu_0 R^3 M_0^2}{\pi d^7}. \tag{5}$$

Figure 5 shows the spatial dependence of the force according to Eq. (4) (black squares) and Eq. (5) (solid black line) assuming $\mu_r \gg 1$. As clear from the figure, our simple model is in very good agreement with the direct measurement of the force.

Establishing a theoretical expression of the magnetic field created by the magnet and channeled through one or two balls in front of the magnet ($n = 1$, 2 in Fig. 5) is beyond the scope of the present article. However, Fig. 5 shows that the estimate of the magnetic force given in Eq. (4) is in reasonable agreement with the direct measurement.

### B. Conversion of magnetic energy into kinetic energy

The available magnetic energy in the presence of $n$ steel balls in front of the magnet are computed from the above spatial dependence of the magnetic force as $\int_{-\infty}^{-2(n+1)R} F_M(x)\,dx$, where the upper limit of the integral is the minimum approaching distance of the center of the incoming ball from the center of the magnet. This magnetic energy be found either by (i) integrating the measured force profile, or (ii) integrating the force expressed as a function of the gradient $B^2$ according to Eq. (4), which leads to $U_n = 4\pi R^3 B^2 [2(n+1)R]/\mu_0$. Table I summarizes the available magnetic energy according to these computations for $n = 0$, 1, and 2. As expected from Sec. II A, a very good agreement is observed between these values, and the available magnetic energy can be conveniently computed from the magnetic field measurement.

Note that a third computation of $U_n$ can also be performed by integrating Eq. (5) when $n = 0$, giving $U_0 = \mu_0 M_0^2/64\pi R^3 = 95 \pm 5$ mJ. This higher estimate can be understood from the slight overestimation of the magnetic field in the vicinity of the magnet using the dipolar approximation. Since most of the acceleration occurs very close to the magnet, this leads to an overestimate of 25% of the available magnetic energy. However, as shown below, the expression of the force given in Eq. (5) is useful to predict the time evolution of the speed of the impacting ball.

A partial conclusion can be drawn here for the optimization of the magnetic cannon. Acceleration in the attraction phase and deceleration in the ejection phase is controlled by the magnetic energies $U_n$ and $U_{m-1}$, which represent, respectively, the loss and gain of magnetic (potential) energy (and resulting in the gain and loss of kinetic energy, respectively). As $U_n$ strongly decreases with $n$, the maximum increase of kinetic energy is achieved for the lowest value of $n$ (i.e., $n = 0$), while the minimum losses are obtained for large values of $m - 1$. The optimization of the number $m$ of balls behind the magnet depends on competing effects between reducing $U_{m-1}$ and reducing the transfer losses within the chain during the soliton propagation. This issue will be addressed in Sec. IV.

Let us now consider the conversion of the available magnetic energy $U_n$ into kinetic energy. The incoming ball is subject to magnetic, friction, and drag forces. However, both friction and drag forces may be neglected; the magnetic force is on the order of 10 N while for $M = 28$-g balls and a maximum velocity of the order of 3 m/s the friction force is estimated to be around 0.03 N and the viscous drag force around $10^{-4}$ N. Because the magnetic force strongly increases as the distance between the incoming ball and the magnet decreases, most of the acceleration occurs in close vicinity of the magnet. As a consequence, the magnetic energy is mostly converted into translational energy and the rotation of the incoming ball can be neglected.

The work-energy theorem leads to a simple expression for the ball velocity $\dot{x}$ given by

$$\dot{x}(x) = \sqrt{\frac{2}{M}\int_{-\infty}^{x} \vec{F}_M \cdot \mathrm{d}\vec{x} + \dot{x}_{-\infty}^2}, \tag{6}$$

where $\dot{x}_{-\infty}$ is the initial velocity at large distance from the magnet (the initial velocity being null in the case of a single cannon, but may be non-zero when several successive rifles are investigated). At impact, this expression reads $K_{\mathrm{impact}} = K_{\mathrm{init}} + U_n$ (i.e., full conversion of the available potential energy into kinetic energy).

The assumptions leading to this simplified expression have been experimentally verified with $n = 0$ and $\dot{x}_{-\infty} = 0$. A high-speed camera (8000 fps) images the incoming ball during the acceleration phase. The velocity of the ball is computed as the derivative of the position of the center of the ball, extracted using ImageJ, a freely available image-analysis program developed by NIH. Figure 6 displays the experimental velocity of the ball (dots) and the theoretical curve (solid line) predicted in Eq. (6) using the dipole approximation of Eq. (5). The impact velocity computed from the integration of the direct force measurement (and assuming a complete conversion of magnetic energy into kinetic energy) is also displayed as the diamond symbol in the figure. The good agreement of the measured final velocity with these estimates shows that friction and drag may indeed be neglected and that the available magnetic energy is fully converted into translational kinetic energy. The curve in Fig. 6 shows that the permanent/induced dipole hypothesis enables us to correctly predict the evolution of the impacting ball velocity; however, this model slightly overestimates the velocity, as expected from the overestimate of the available magnetic energy discussed above.

Table I. Available magnetic energy estimated from direct magnetic force measurement, or from a permanent/induced model involving the direct magnetic field measurement. The larger errors reported in the right column lie in the low spatial resolution of the direct magnetic field measurements.

| $n$ | $U_n$ (mJ) (from measured force) | [from Eq. (4)] |
|---|---|---|
| 0 | $72 \pm 3$ | $75 \pm 25$ |
| 1 | $7.2 \pm 1$ | $6.4 \pm 1$ |
| 2 | $1.4 \pm 0.2$ | $1.6 \pm 0.4$ |

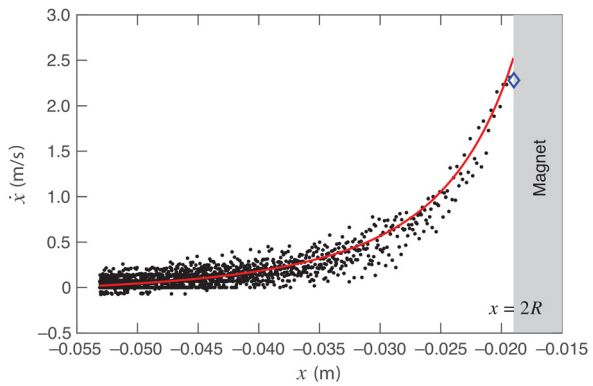


Fig. 6. Spatial dependence of the incoming ball velocity ($n = 0$): experimental values obtained using video analysis (dots), permanent/induced model (solid curve), and final velocity estimated from integration of the magnetic force measurement, assuming a complete conversion of magnetic energy into kinetic energy (diamond).

As a partial conclusion here, we showed that the available magnetic energy from the attraction of the magnet is fully converted into translational kinetic energy. Moreover, we provided a simplified expression of the force exerted by the magnet on the steel ball that leads to a theoretical expression of the magnetic energy $U_n$. Similar arguments can be applied for the ejection phase, where the kinetic energy of the ejected ball is given by $K_{\text{final}} = K_{\text{eject}} - U_{m-1}$.

## III. NESTERENKO SOLITON: FROM NEWTON'S CRADLE TO GAUSS CRADLE

Following the impact of the incoming steel ball, the energy propagates in the ball chain similarly to what occurs in Newton's cradle.[12,13] However, in the magnetic cannon, the chain is inhomogeneous due to the presence of a sintered NdFeB magnet. This section develops a classical model based on Hertzian contact and discusses briefly the Nesterenko soliton. Experimental data accounting for the presence of the magnet are then presented.

### A. Nesterenko soliton: Propagation of a non-linear wave

Let us consider a chain of $N$ balls of radius $R$ allowed to translate along the $x$-axis and let the positions of the balls be given by $x_i$, as shown in Fig. 7(a). The force acting between two balls in contact is given by the Hertz law[19]

$$F = \frac{E\sqrt{2R}}{3(1-\nu^2)}(x_i - x_{i+1} - 2R)^{3/2}, \tag{7}$$

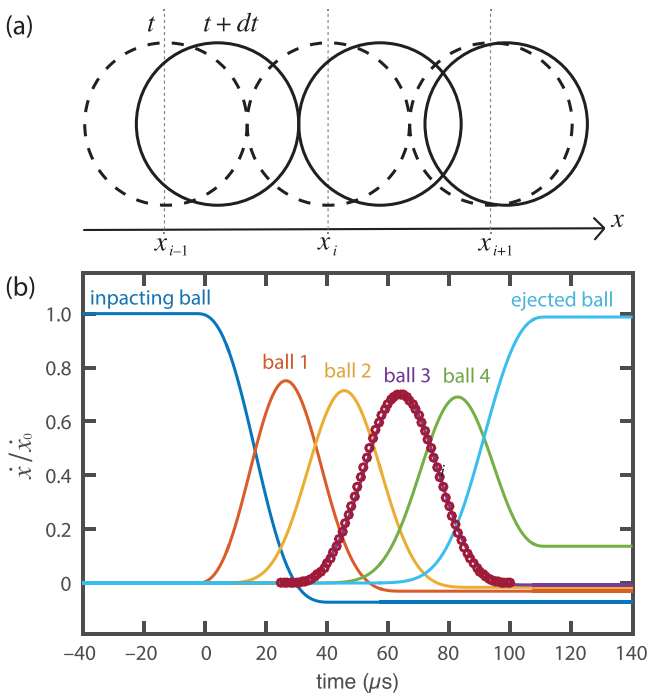


Fig. 7. (a) Sketch of the geometry of the chain of balls. At time $t$, the balls—dashed circles—are centered at locations $x_{i-1}(t), x_i(t), x_i(t)$. At time $t+dt$, each ball, now represented by a solid circle, experienced a move towards the right, and possibly compression as between ball $i$ and $i+1$. (b) Time evolution of the velocity of each ball normalized by the velocity of the incoming ball. The last ball is ejected at a slightly lower speed than any of the other balls. The open circles represent the analytic solution of the solitary wave.

with $E$ and $\nu$ being, respectively, the Young and Poisson moduli of the ball material.

In the case of the steel balls used in our experiments, an upper bound of the compression $\delta = x_i - x_{i+1} - 2R$ of the balls during the propagation of the wave can be estimated assuming equality of the compression energy $2E\sqrt{2R}\delta^{5/2}/[15(1-\nu^2)]$ with the kinetic energy of the impacting ball (on the order of 0.05 J). The corresponding force is on the order of 1000 N, which largely exceeds the magnetic force experienced by the steel balls (even when in direct contact with the magnet, typically 25 N). Such a large compression force demonstrates that the properties of the solitary compression wave are unaffected by the magnetic forces acting within the chain (although obviously the velocity of the impact ball strongly depends on the magnetic force).

Knowing the forces acting on each ball, the equations of motion can be numerically solved. Figure 7(b) shows the numerical solution for a chain of five steel balls ($E = 210$ GPa, $\nu = 0.3$) of radius $R = 9.5$ mm. This graph shows several interesting features. First, the final velocity of the impacting ball is negative, meaning it experiences a rebound (note that, unlike in the experiments, the first ball of the chain is unconstrained). Second, the final velocity of the second-to-last ball is non-zero (although small), showing that several balls can be ejected. (These features are also visible in an actual Newton's cradle.) Third, since in this simple case the total energy is conserved, the velocity of the last ball is (slightly) less than that of the impacting ball ($v_{\text{eject}} \approx 0.987 v_{\text{impact}}$). The main conclusion is therefore that, even without any dissipation, the transmitted energy of the ejected ball $K_{\text{eject}}$ is lower than the kinetic energy of the impacting ball $K_{\text{impact}}$ and a yield $\eta = K_{\text{eject}}/K_{\text{impact}}$ should be introduced. For the specific case displayed in Fig. 7(b), the numerical simulation provides an estimate of $\eta = 0.975$.

As a side note, it is worth mentioning that an analytic, solitary, traveling-wave solution to the continuous limit of the equation of motion was given by Nesterenko to be[20,21]

$$\frac{\partial x}{\partial t} = A \sin^4\left(\frac{x - ct}{L}\right), \tag{8}$$

where $c$ is the speed of the wave and $L$ is a measure of its spatial extent. This analytic solution is in excellent agreement with the numerical solution (see Fig. 7). Remarkably, the dispersion is counter-balanced by the non-linearities and this solitary wave travels without distortion. Among other interesting features, it should be mentioned that the spatial extension of the soliton is constant ($L \simeq 10R$) while its velocity $c$ increases with increasing amplitude $A$. The duration of the propagation for a given chain therefore decreases with increasing velocity of the impacting ball.

### B. Experimental measurement of the energy transmission yield $\eta$

The above model does not account for any source of energy dissipation. An experimental determination of the yield $\eta = K_{\text{eject}}/K_{\text{impact}}$ is required to derive a global energy balance of the magnetic cannon. Figure 8(a) shows the experimental setup used. The energy of the impacting ball is controlled via the launching height of a pendulum hitting the chain (with no magnet), and the energy of the ejected ball is computed from its impact position on the ground after falling from a table. Similar to the above mentioned model, none of

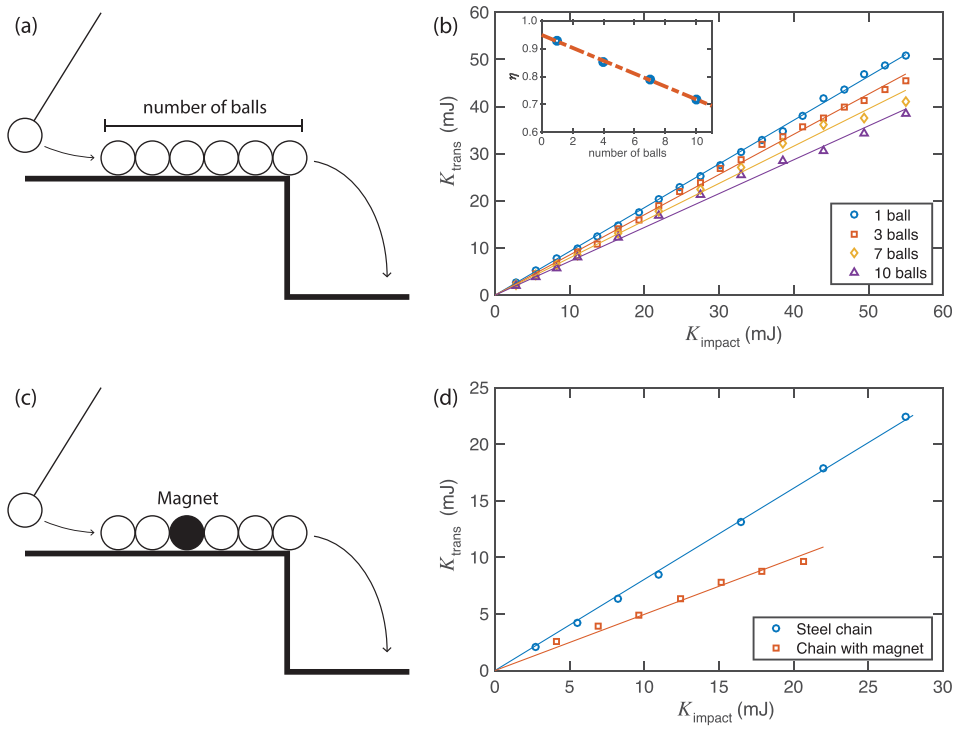


Fig. 8. (a) Diagram representing the setup for the energetic yield of the chain. The impacting energy is controlled thanks to a pendulum and the ejected energy is measured after a fall. (b) Energy of the ejected ball as a function of the energy of the impacting ball for different chain lengths without magnet. (c) Diagram representing the setup for the energetic yield of the chain with a magnet. (d) Energy of the ejected ball as a function of the energy of the impacting ball for a five-ball chain with and without a magnet.

the balls are fixed. Figure 8(b) shows the measurements of the energy transmitted to the ejected ball $K_{\text{eject}}$ as a function of $K_{\text{impact}}$. Several interesting features should be emphasized. First, the energy transmitted to the ejected ball is proportional to the energy of the impacting ball. Second, the yield $\eta$ decreases with the length of the chain. And third, the experimental yield is lower than 0.975 due to numerous sources of dissipation (for a chain of five balls the experimental yield is only about 0.83). The experimental determination of the yield is compatible with a linear function $\eta = \eta_0 - 0.024\,(n+m+1)$, with $\eta_0 = 0.95$ in the case of a chain of steel balls. This result shows that source of dissipation (viscous and solid friction, deformations or imperfect contacts between the balls in the chain) cannot be neglected.

In the magnetic cannon, the presence of the magnet not only introduces an inhomogeneity, but it also introduces a magnetic field that magnetizes the steel balls, leading to a strong attraction between the balls (thus preventing, for instance, the rebound of the impacting ball). The strength of the magnetic field does not modify the physical principles at play in the Nesterenko soliton propagation, as the maximum intensity of the magnetic force for a 600-mT field is three orders of magnitude below the mechanical compression forces. Moreover, the NdFeB magnet introduces an inhomogeneity with distinct mechanical properties (Young and Poisson moduli, as well as density) that may cause a higher dissipation due to its sintered structure. The presence of an intruder (the magnet) in the chain also triggers a partial reflection of the wave. This partial reflection leads to momentum propagation in the $-x$ direction that could lead to a recoil of the chain containing the magnet if the latter is not held to the rail (such a recoil is not observed in our experiment since the magnet is tightly held to the rail with putty, as shown in Fig. 1).

In order to estimate the global effective dissipation for the magnetic cannon, the experimental setup is modified as shown in Fig. 8(c). The data in Fig. 8(d) show the transmitted kinetic $K_{\text{trans}}$ as a function of the impacting kinetic energy $K_{\text{impact}}$ for a seven-ball chain, with and without a magnet. Note that the increase/decrease of energy from magnetic acceleration/deceleration has been taken into account in the computation of the energies. Yet, the insertion of the magnet leads to an impressive yield drop from 81% to 44%, resulting in a value of $\eta_0 \sim 0.61$.

## IV. OPTIMIZATION OF THE MAGNETIC CANNON

### A. Optimization of a single magnetic cannon

As previously stated, the optimal energy gain is obtained with no ball on the left of the magnet ($n=0$), and depends strongly on the properties of the magnet. The optimal configuration also requires minimizing the loss of kinetic energy in the ejection phase, or, equivalently, minimizing the magnetic energy $U_{m-1}$, which is accomplished by using a large number of balls on the right of the magnet ($m \gg 1$). At the same time, we want to maximize the yield $\eta$ of the chain, which requires minimizing the total number $m+n+1$ of balls in the chain. The details provided in Secs. II–III enable us to express the kinetic energy of the ejected ball as a function of the initial kinetic energy and the properties of the system as

$$K_{\text{final}} = \eta(n+m+1)[K_{\text{init}} + U_n] - U_{m-1}. \tag{9}$$

The maximal value of $K_{\text{final}}$ is obtained when the total losses $[1-\eta(n+m+1)]U_n + U_{m-1}$ are minimized. Figure 9 shows the normalized losses as a function of $m$ for $n=0$ (in this configuration, no ball is ejected when $m=1$). A weak

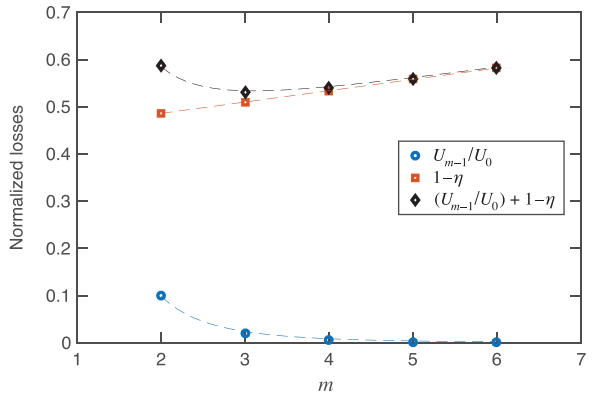


Fig. 9. Energy losses, normalized to $U_0$, as a function of $m$: magnetic energy (circles), loss within the chain (squares), and total losses (diamonds).

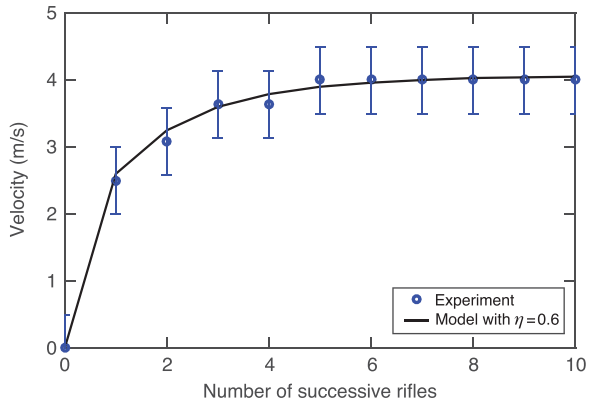


Fig. 10. Time-averaged velocity of balls ejected by successive identical rifles (estimated from sound recording) and model (solid line) with $\eta = 0.6$.

minimum is observed for $m=3$, and for $m>3$ the losses slowly increase with $m$. This figure shows that the magnetic energy $U_{m-1}$ can be neglected in the losses when $m > n+2$. The optimal configuration, which maximizes the kinetic energy of the ejected ball, is thus obtained when no balls are in front of the magnet, and three balls are behind the magnet ($n=0$, $m=3$), which is the configuration displayed in Fig. 1.

The kinetic energy of the ejected ball is most conveniently expressed when neglecting $U_{m-1}$ in Eq. (9). The dipolar moment of the magnet can be estimated as $M_0 \sim 4\pi R^3 B_r/3\mu_0$, with $B_r$ the residual flux density (on the order of 1.27 T for a grade N40 NdFeB magnet), which leads to

$$K_{\text{final}} \sim \left[\eta_0 - 0.024(m+1)\right]\frac{\pi R^3 B_r^2}{36\mu_0}. \tag{10}$$

### B. Maximal acceleration achievable using $N$ successive rifles

Once the optimization of a single magnetic rifle has been achieved, a natural question arises: to what extent is it possible to increase the ejected kinetic energy by using a succession of several rifles?

Let us now focus on a configuration with $N$ successive identical magnetic rifles, where the ball ejected from rifle $i$ will be accelerated by rifle $i+1$ according to Eq. (9). When neglecting losses between two successive rifles, the kinetic energy of the last ejected ball reads

$$K_{\text{final}}(N) = \eta^N U_{\text{init}}^0 + U_n \sum_{i=1}^{N} \eta^i - U_{m-1} \sum_{i=0}^{N-1} \eta^i. \tag{11}$$

The kinetic energy of the ejected ball increases with the number of modules. Since the energy gain is constant and independent of the initial velocity, while the dominant source of energy losses (through the propagation of the soliton within the chain) is proportional to the impacting energy, there is a maximum achievable kinetic energy of

$$K^{\max} = \frac{\eta U_n - U_{m-1}}{1-\eta}. \tag{12}$$

This saturation has been experimentally observed using a chain of ten rifles composed of one magnet followed by $m=3$ balls and separated by 10 cm (note that for this specific setup, the balls have a radius of 4 mm). The velocities of the ejected balls were estimated from sound recording of the successive shocks between the ball ejected from rifle $i$ and the magnet of rifle $i+1$ and is displayed in Fig. 10. This low-cost technique provides a simple method of obtaining the time-averaged velocity between two successive rifles. The experimental results are consistent with the prediction given above, neglecting $U_{m-1}$, using $U_0$ as determined by the direct force measurement and a yield $\eta = 0.6$.

## V. CONCLUSION

In conclusion, we were able to successfully model the kinetic energy of the ball ejected from a magnetic cannon. In the acceleration phase, the experimental data shows a very good agreement with a simple model of uniform magnetization of a sphere in the magnetic field created by the magnet. In the case where no steel balls are present between the incoming ball and the magnet, this magnetic field is accurately modeled as a dipolar magnetic field. We also provided a model based on Hertzian contact and solid collisions accounting for the propagation of momentum in the chain of balls and experimental determined an effective yield accounting for its efficiency. These ingredients enable us to predict the final kinetic energy as a function of the parameters of the system (geometrical sizes, magnetic properties) for a single magnetic cannon or an assembly of several modules.

Some limitations in this work could benefit from further analysis and modeling. In the presence of steel balls between the magnet and the incoming ball ($n \geq 1$), we derived the magnetic force as a function of the spatial dependence of the magnetic field. However, a detailed modeling of the "channeling" of the dipolar field created by the magnet within ferromagnetic balls would make it possible to predict more precisely the energy gain in the acceleration phase. The study of the behavior of the magnetic cannon using paramagnetic or super-paramagnetic materials instead of ferromagnetic materials could also be envisioned. The modeling of momentum propagation described in the present article is very similar to the Newton's cradle. Including the cohesion forces from the magnetic field as well as an effective behavior of the sintered NdFeB magnet could also be an extension of this work.

## ACKNOWLEDGMENTS

This work was supported by the École Normale Supérieure de Lyon and Univ Claude Bernard, Lyon, France.

The authors acknowledge also A. Bourges, C. Gouiller, A. Guittonneau, C. Malciu, G. Panel, and J. Sautel with whom discussions and exchanges were prolific. The authors would like to emphasize that the work presented here was done in preparation for the International Physicists Tournament (Ref. 22), a world-wide competition for undergraduate students. The authors would highly recommend participation in the IPT as a rare learning opportunity for undergraduate students. The organization committee of the International Physicist Tournament is gratefully acknowledged, as are contributions of the French Academy of Sciences and all the other tournament's partners.

[a]Electronic mail: nicolas.plihon@ens-lyon.fr

[1]J. A. Rabchuk, "The Gauss rifle and magnetic energy," Phys. Teach. **41**(3), 158–161 (2003).
[2]D. Kagan, "Energy and momentum in the gauss accelerator," Phys. Teach. **42**(1), 24–26 (2004).
[3]O. Chittasirinuwat, T. Kruatong, and B. Paosawatyanyong, "More fun and curiosity with magnetic guns in the classroom," Phys. Educ. **46**(3), 318–322 (2011).
[4]C. Ucke and H.-J. Schlichting, "Die magnetkanone," Phys. Unserer Zeit **40**(3), 152–155 (2009).
[5]S. O. Starr, R. C. Youngquist, and R. B. Cox, "A low voltage railgun," Am. J. Phys. **81**(1), 38–43 (2013).
[6]R. Castañer, J. M. Medina, and M. J. Cuesta-Bolao, "The magnetic dipole interaction as measured by spring dynamometers," Am. J. Phys. **74**(6), 510–513 (2006).
[7]N. Derby and S. Olbert, "Cylindrical magnets and ideal solenoids," Am. J. Phys. **78**(3), 229–235 (2010).
[8]R. S. Davis, "Using small, rare-earth magnets to study the susceptibility of feebly magnetic metals," Am. J. Phys. **60**(4), 365–370 (1992).
[9]B. S. N. Prasad, S. V. Shastry, and K. M. Hebbar, "An experiment to determine the relative permeability of ferrites," Am. J. Phys. **40**(6), 907–910 (1972).
[10]J. F. Borin and O. Baffa, "Measuring magnetic properties of ferromagnetic materials," Am. J. Phys. **66**(5), 449–452 (1998).
[11]W. M. Saslow, "How a superconductor supports a magnet, how magnetically soft iron attracts a magnet, and eddy currents for the uninitiated," Am. J. Phys. **59**(1), 16–25 (1991).
[12]F. Herrmann and M. Seitz, "How does the ball-chain work?," Am. J. Phys. **50**(11), 977–981 (1982).
[13]S. Hutzler, G. Delaney, D. Weaire, and F. MacLeod, "Rocking Newton's cradle," Am. J. Phys. **72**(12), 1508–1516 (2004).
[14]D. Gugan, "Inelastic collision and the Hertz theory of impact," Am. J. Phys. **68**(10), 920–924 (2000).
[15]D. J. Griffiths, *Introduction to Electrodynamics*, 4th ed. (Pearson, Boston, MA, 2013), pp. 373–381.
[16]J. D. Jackson, *Classical Electrodynamics*, 3rd ed. (John Wiley & Sons, New York, NY, 1998).
[17]D. P. Jackson, "Dancing paperclips and the geometric influence on magnetization: A surprising result," Am. J. Phys. **74**(4), 272–279 (2006).
[18]There are a number of affordable linear Hall effect sensors such as AD22151 from Analog Devices, A1302 from Allegro Microsystems, HAL401 from Micronas, or SS39/SS49 from Honeywell.
[19]H. Hertz, "On the contact of elastic solids," J. Reine Angew. Math. **92**, 156–171 (1882).
[20]S. Sen and M. Manciu, "Discrete Hertzian chains and solitons," Physica A **268**(3–4), 644–649 (1999).
[21]V. F. Nesterenko, "Propagation of nonlinear compression pulses in granular media," J. Appl. Mech. Tech. Phys. **24**(5), 733–743 (1983).
[22]More information on the International Physicists Tournament (IPT) can be found at < http://iptnet.info >. Each national team is composed of six students who work throughout the academic year on a list of seventeen open questions and present their findings during the tournament. Unlike a typical physics exam, the problems must not only be presented, but also challenged and reviewed by the other participants, allowing students to respectively assume the roles of researchers, referees, and editors. In addition to the challenge that the tournament represents, it provides students with an exciting and eye-opening experience in which they learn how to design experiments with the aim of solving physics problems, and to constructively criticize scientific solutions.

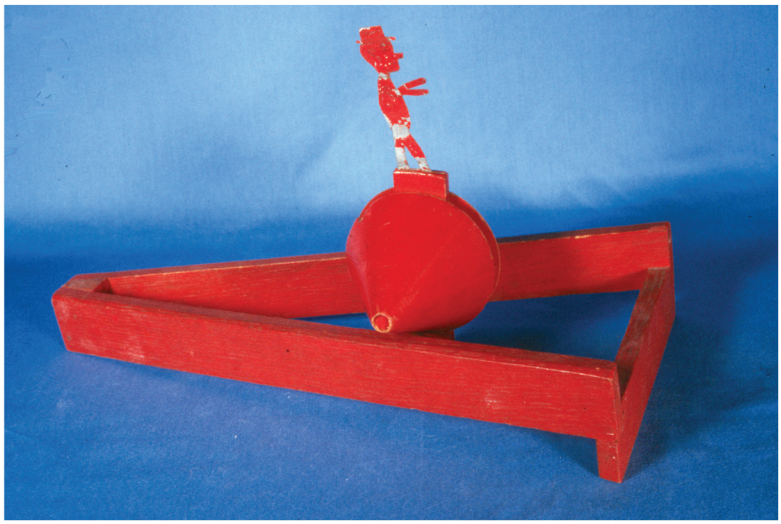

**Cone Rolling Uphill**

This demonstration of a pair of cones rolling uphill was probably made by Prof. Elbe H. Johnson of Kenyon College in the 1920s, and has always seemed to be on the cusp between physics and folk art. The metal figure of the man with a hat rides freely on an axle that connects the two cones. He is counterweighted so that he is always upright. When the system is started at the left-hand side, it moves steadily in what appears to be the uphill direction. In reality, because of the slopes of the two guide rails and the cones, the center of mass of the system is actually getting lower as the system moves. (Picture and Notes by Thomas B. Greenslade, Jr., Kenyon College)